

# TESLA-X: An effective method to search for sub-threshold lensed gravitational waves with a targeted population model

Alvin K. Y. Li,<sup>1, a</sup> Juno C. L. Chan,<sup>2, b</sup> Heather Fong,<sup>3, 4, 5, c</sup> Aidan H.Y. Chong,<sup>6</sup> Alan J. Weinstein,<sup>1</sup> and Jose M. Ezquiaga<sup>2</sup>

<sup>1</sup>*LIGO Laboratory, California Institute of Technology, Pasadena, CA 91125, USA*

<sup>2</sup>*Niels Bohr International Academy, Niels Bohr Institute, Blegdamsvej 17, 2100 Copenhagen, Denmark*

<sup>3</sup>*RESCEU, The University of Tokyo, Tokyo, 113-0033, Japan*

<sup>4</sup>*Graduate School of Science, The University of Tokyo, Tokyo 113-0033, Japan*

<sup>5</sup>*University of British Columbia, Vancouver Campus, Vancouver, B.C. V6T 1Z4, 2329 West Mall, Canada*

<sup>6</sup>*Department of Physics, The Chinese University of Hong Kong, Hong Kong*

(Dated: June 6, 2024)

Strong gravitational lensing can produce copies of gravitational-wave signals from the same source with the same waveform morphologies but different amplitudes and arrival times. Some of these strongly-lensed gravitational-wave signals can be demagnified and become sub-threshold. We present TESLA-X, an enhanced approach to the original GstLAL-based TargetEd Subthreshold Lensing seArch (TESLA) method, for improving the detection efficiency of these potential sub-threshold lensed signals. TESLA-X utilizes lensed injections to generate a targeted population model and a targeted template bank. We compare the performance of a full template bank search, TESLA, and TESLA-X methods via a simulation campaign, and demonstrate the performance of TESLA-X in recovering lensed injections, particularly targeting a mock event. Our results show that the TESLA-X method achieves a maximum of  $\sim 10\%$  higher search sensitivity compared to the TESLA method within the sub-threshold regime, presenting a step towards detecting the first lensed gravitational wave. TESLA-X will be employed for the LIGO-Virgo-KAGRA's collaboration-wide analysis to search for lensing signatures in the fourth observing run.

## I. INTRODUCTION

Gravitational lensing refers to the phenomenon in which properties of propagating waves are influenced by the distortion of spacetime caused by massive intervening objects. The effects of gravitational lensing depends on the mass properties of the lens [1–6]. For massive lenses significantly larger than the gravitational-wave wavelength, we can assume geometric optics, which results in repeated signals with relative (de-)magnifications, time delays, and phase shifts [4, 7–17]. Lenses with sizes comparable to gravitational-wave wavelengths can produce beating patterns through frequency-dependent wave optics effects, formally known as microlensing [3, 5, 6, 18–28].

The search for gravitationally-lensed gravitational waves is driven by various scientific objectives, such as testing general relativity [8, 29–32], improving source localization accuracy [33, 34], characterizing lens models [19, 22, 35, 36], and performing precision cosmology [33, 37–39] and statistical cosmology [40].

The LIGO-Virgo-KAGRA (LVK) collaboration has conducted various analyses searching for lensing signatures in the event catalogs of LVK's observing runs O1-O2 [41] and O3 [42, 43], but no convincing evidence of lensing signatures has been found. Additionally, other analyses have concluded that there are no confident lensing signatures in the detected gravitational-wave events [17, 44–47].

Strongly lensed gravitational waves will likely originate from sources living in the higher redshift universe. With-

out being lensed, these signals will only be barely detectable or undetectable. Under strong lensing, copies of gravitational waves from these high redshift sources will be produced; some may be magnified and are detected as super-threshold gravitational waves, but some may be potentially de-magnified with a reduced signal-to-noise (SNR) ratio below the detection threshold. These signals, formally known as “sub-threshold” signals, are of particular interest, as a significant proportion of strongly-lensed gravitational-wave events falls into this category [48]. Retrieving these possible sub-threshold lensed counterparts is a crucial step in boosting confidence for the first detection of strongly-lensed gravitational waves.

Two targeted search methods [44, 45] have been developed and employed to recover potential sub-threshold lensed counterparts to known super-threshold gravitational waves. The GstLAL-based TargetEd Subthreshold Lensing seArch (TESLA) described in [44] strategically reduces the search parameter space to look for possible sub-threshold lensed counterparts. However, as we will explain in this paper, the traditional TESLA method can potentially lose signals due to an excessive loss in signal-to-noise (SNR) ratio due to how the targeted template bank is constructed.

Additionally, TESLA's efficiency in finding potential sub-threshold lensed gravitational waves can be improved if a targeted population model built based on information from the target superthreshold event is used. A proper targeted population model in the ranking statistic can further reduce the influence of the noise background. Detailed information on the TESLA method can be found in [44].

In this paper, we present a novel method, TESLA-X, to search for strongly-lensed sub-threshold gravitational-wave signals. TESLA-X employs a targeted population model to enhance the search sensitivity for potential lensed sub-

<sup>a</sup> kli7@caltech.edu

<sup>b</sup> chun.lung.chan@nbi.ku.dk

<sup>c</sup> hkyfong@gmail.com

threshold signals, and it addresses the excessive SNR loss issue by utilizing a new targeted template bank construction method.

This paper is organized as follows: Section II provides a brief review of strong lensing of gravitational waves. Section III outlines the workflow of the traditional TESLA method. In Section IV, we give an overview of how the population prior term in the likelihood ratio calculations for triggers from the GstLAL search pipeline is calculated, and detail the TESLA-X methodology. Section V presents a simulation campaign to evaluate the TESLA-X method. Finally, in Section VI, we summarize our findings and discuss potential future work to further enhance the search sensitivity of the TESLA-X pipeline.

## II. STRONG LENSING OF GRAVITATIONAL WAVES

Massive objects, like galaxies and galaxy clusters, can produce distortion in spacetime. General relativity predicts that when waves emitted from a source pass by these massive objects (also known as *gravitational lenses*), they will be deflected due to the curvature of spacetime. This effect is known as *gravitational lensing*, which is universal according to the equivalence principle, i.e. it affects gravitational waves in the exact same way as electromagnetic waves (EM waves). Depending on the spatial extent of the potential well of gravitational lenses and the scales of wavelength, the effect of gravitational lensing can be vastly different. In fact, gravitational lensing can be sub-classified into strong lensing, weak lensing, and microlensing. Some literature also distinguishes millilensing as a sub-type of gravitational lensing. In this paper, we focus on *strong lensing* with geometric optics, in which we assume that gravitational waves have a much shorter wavelength than the spatial scale of the gravitational lenses.

Under the strong lensing hypothesis, strong gravitational lenses can produce multiple copies of transient gravitational waves from the same source. These repeated signals have identical waveforms (i.e. their underlying intrinsic parameters  $\vec{\theta}$ , e.g. component masses and spins, are the same), except that (I) their amplitudes may differ by some amplitude scaling factor  $\sqrt{\mu_j}$  (Note that the amplitude scaling factor is achromatic under the geometric optics assumption, and the amplification factor can be  $> 1$  (magnified) or  $\leq 1$  (de-magnified).), (II) they are separated by a relative arrival time delay  $\Delta t_j$  with respect to the not-lensed signal's coalescence time, and (III) they have an additional Morse phase factor  $\Delta\phi_j$  applied to depending on the type of lensed signals (Note: There are three types of lensed signals, type I, II and III. They correspond to the minimum, saddle point, and maximum time-delay solution to the lens equation, respectively.), given by [29, 46]

$$\Delta\phi_j = -\frac{n_j\pi}{2}, \quad n_j = \begin{cases} 0, & \text{Type I lensed signals} \\ 1, & \text{Type II lensed signals} \\ 2, & \text{Type III lensed signals} \end{cases}. \quad (1)$$

Mathematically, if we denote the not-lensed gravitational wave in the frequency domain as  $\tilde{h}^{\text{NL}}(f; \vec{\theta}, \Delta t_j = 0)$ , then

the  $j^{\text{th}}$  strongly-lensed counterpart waveform  $\tilde{h}_j$  is

$$\tilde{h}_j(f; \vec{\theta}, \mu_j, \Delta t_j, \Delta\phi_j) = \sqrt{|\mu_j|} \tilde{h}^{\text{NL}}(f; \vec{\theta}, \Delta t_j) e^{(i \text{sign}(f) \Delta\phi_j)}. \quad (2)$$

Since the travelling paths of these repeated signals have been altered, these signals will appear to be originating from sources at different sky locations. However, the deviation in sky location due to strong lensing is in order of arc-seconds. This is negligible compared to the uncertainty in sky localization for gravitational waves, which is in the order of degrees [49]. Therefore, for the rest of this paper we will assume multiple strongly-lensed gravitational-wave signals from the same source to have the same sky location.

## III. THE SEARCH FOR SUB-THRESHOLD STRONGLY-LENSED GRAVITATIONAL WAVES: OBJECTIVES AND CURRENT APPROACH

### A. Current effort to search for strongly-lensed sub-threshold lensed counterparts to super-threshold gravitational waves

When searching for gravitational waves in general, signals with sufficiently high amplitudes that can be identified as gravitational waves from the noisy data are known as *super-threshold*. In contrast, weaker gravitational waves not distinguishable from noise are known as *sub-threshold*. As discussed in Section II, strong lensing can produce multiple copies of gravitational waves coming from the same source with different amplification factors  $\sqrt{\mu_j}$ .  $\sqrt{\mu_j}$  can take on values smaller than 1, i.e. the repeated gravitational-wave signals are *de-magnified* compared to the not-lensed gravitational-wave signal and may become sub-threshold. It is then natural to ask the question: If we assume that one of the identified super-threshold gravitational waves detected so far is strongly lensed, can we find its sub-threshold strongly lensed counterparts, if they exist?

There have been ongoing efforts to employ *matched-filtering based search pipelines* with modifications [44, 45] to search for strongly-lensed sub-threshold lensed counterparts to identified super-threshold gravitational waves from LVK's first three observing runs (O1, O2 and O3) [41–43]. In this paper, we focus on the *TargetEd subthreshold Lensing seArch (TESLA)* method [44], which is built based on the GstLAL search pipeline [50–58]. The following sub-section gives a brief introduction to the traditional TESLA method.

### B. The traditional TESLA search method

Traditional TESLA is built based on the matched-filtering-based pipeline GstLAL. A detailed introduction to the GstLAL search pipeline can be found in [44, 50, 54]. In a general search for gravitational waves from compact binary coalescences, the goal is to detect signals that span the entire parameter space to which the detector network's frequency bandwidth is sensitive. Hence, a large template bank comprising over a million template waveforms is constructed and used. A

large number of candidates (also known as triggers) is generated, regardless of whether they are noise or signals. The more templates we use in a search, the larger the trials factor, and hence, the larger the noise background will become.

Gravitational waves with weaker amplitudes, for instance, strongly-lensed sub-threshold lensed counterparts, can be buried in the large noise background. Hence, it is necessary to tactically reduce the noise background while keeping the targeted foreground constant to uncover possible weaker gravitational waves.

Assuming a super-threshold gravitational wave is strongly lensed, we want to search for its possible sub-threshold lensed counterparts. In section II, we explained that strongly-lensed gravitational waves from the same source should have identical intrinsic parameters (e.g. component masses and spins), and hence identical waveforms. For each super-threshold event (target), we obtain the posterior probability distribution that gives the best estimates of the source parameters of the target using the Bayesian parameter estimation analyses described in [59–62]. We can then narrow down the parameter search space for possible strongly-lensed sub-threshold counterparts to regions consistent with the target’s posterior parameter space. However, as explained in [44], the posterior parameter space of the target itself is insufficient because of noise fluctuations in the data. Non-Gaussianity in the data can cause false signals (especially those that have weaker amplitudes and are hence sub-threshold), to be registered by templates that have very different parameters than those of the posterior samples for the target.

TESLA accounts for both the signal sub-space and noise fluctuations in the data when searching for possible strongly-lensed sub-threshold counterparts to super-threshold gravitational waves. Here, we outline the steps for running a TESLA analysis. For each super-threshold gravitational event (target), we start with the posterior samples ordered in decreasing order of log-likelihood from the parameter estimation for the target. Since the amplitudes of possible strongly-lensed sub-threshold gravitational waves are lower, they will be registered as triggers in the search pipeline with lower signal-to-noise ratio  $\rho$  (SNR). For each posterior sample, we generate 1 injection with the exact same parameters (including luminosity distance to the source  $D_L$  and sky location, i.e. right ascension  $\alpha$  and declination  $\delta$ ) as the sample, and 9 extra injections with  $D_L$  increased (and hence optimal SNR  $\rho_{\text{opt}}$  decreased) to mimic the de-magnifying effect of strong lensing on the amplitudes of possible sub-threshold lensed counterparts, according to the inverse proportionality of  $D_L$  and the optimal SNR  $\rho_{\text{opt}}$ :

$$D_L \propto \frac{1}{\rho_{\text{opt}}}. \quad (3)$$

We require the latter 9 injections to have detector SNR  $\rho_{\text{det}} \geq 4$  in at least one detector as a constraint from the GstLAL search pipeline (Note: We do not lower the single detector SNR threshold in the GstLAL search pipeline since this will lead to an exponential increase in the number of both signal and noise triggers. As future work, we will explore the possibility of further lowering the single detector SNR thresh-

old.). The set of lensed injections represents the possible sub-threshold lensed counterparts to the target we are searching for. They are then injected into real data, and we perform an injection campaign using GstLAL with a full template bank to recover them. After the injection campaign, templates that can find these injections (Note: An injection is “found” if the FAR of the associated trigger is  $\leq 1$  in 30 days.) are kept to construct a targeted template bank to search for possible strongly-lensed sub-threshold counterparts to the target. The end product of TESLA is a ranked list of possible lensed counterparts to the target in increasing order of FARs. Readers are reminded that the FARs (or other ranking statistics) reported in the search’s ranked list do not indicate how likely the signal candidate is a lensed counterpart to the target, but only a priority label for follow-up analysis.

For a detailed explanation of the TESLA method, please refer to [44].

#### IV. THE UPGRADED TESLA-X SEARCH METHOD

##### A. The missing pieces in the traditional TESLA method: Non-optimal template bank and population model

We have shown in [44] that the traditional TESLA method succeeds in improving the search sensitivity to possible strongly-lensed sub-threshold gravitational waves. However, the whole picture still needs to include two puzzle pieces.

First, in the original full template bank, the parameter ranges are informed by the masses and spins of detectable sources (BNS, NSBH, BBH), and the templates are distributed with a density that allows a maximum loss of 3% SNR when a gravitational-wave signal is recovered (compared to the optimal SNR (Note: The optimal SNR is the SNR when the signal is cross-correlated with a template with the exact same parameters as the signal) [57]). However, when a reduced template bank is generated using traditional TESLA, we discard templates that did not recover lensed injections for the target super-threshold gravitational waves. This breaks the original optimality of the full template bank, caused by the finite number of lensed injections that are used to generate the reduced template bank, and strongly-lensed sub-threshold signals whose optimal detector SNR is near threshold (i.e. around  $\rho_{\text{opt}} \approx 4.12$ ) will not be detected. Therefore, it is vital that the optimality of the reduced template bank must be conserved to maximize our search sensitivity towards possible strongly-lensed sub-threshold gravitational waves.

Second, a population model was not set in traditional TESLA. In the analysis, the absence of a population model carries an implicit assumption that every template in the template bank has an equal probability of recovering a possible sub-threshold counterpart. Since our goal is to detect sub-threshold counterparts whose intrinsic parameters are identical to a super-threshold signal, implementing a population model centered around the signal’s recovered parameters will increase the pipeline’s sensitivity in detecting signals in that region. The population model should also be dependent on SNR to account for sub-threshold signals that are coloured by

noise and, thus, could be recovered by a template that is different from that recovered the super-threshold signal.

### B. The likelihood ratio in the GstLAL search pipeline

To rank candidates, GstLAL assigns each trigger a likelihood ratio as its ranking statistic, defined as [50, 51, 54]:

$$\mathcal{L} = \frac{P(\vec{D}_H, \vec{O}, \vec{\rho}, \vec{\xi}^2, [\Delta\vec{t}, \Delta\vec{\phi}] | \vec{\theta}, \text{signal})}{P(\vec{D}_H, \vec{O}, \vec{\rho}, \vec{\xi}^2, [\Delta\vec{t}, \Delta\vec{\phi}] | \vec{\theta}, \text{noise})} \cdot \mathcal{L}(\theta), \quad (4)$$

where the first term,  $P(\dots | \vec{\theta}, \text{signal})/P(\dots | \vec{\theta}, \text{noise})$ , is the ratio of the probability of obtaining the candidate event under the signal model to that under the noise model. It depends on (1) the detectors  $\vec{O}$  that are participating at the time of the candidate event, (2) the horizon distances of the participating detectors  $\vec{D}_H$ , (3) the detector SNRs  $\vec{\rho}$  and (4) The candidate event's auto-correlation-based signal consistency test values at each detector  $\vec{\xi}^2$ . If a candidate event is found in coincidence at multiple detectors (i.e. the event is a *coincident* event),  $\mathcal{L}$  will also include (5) the relative time delays  $\Delta\vec{t}$  and (6) the relative phase delays  $\Delta\vec{\phi}$  of the candidate event between participating detectors (Note: These relative time delays and phase delays should not be confused with the relative time delays and phase delays coming from strong lensing.).

The second term in Equation 4,

$$\mathcal{L}(\theta) = \frac{P(\vec{\theta} | \text{signal})}{P(\vec{\theta} | \text{noise})}, \quad (5)$$

is the ratio of the probability that a trigger is recovered by a template with parameters  $\vec{\theta}$ , given the trigger is an astrophysical signal or noise. Because this ratio does not depend on the data observed by the detectors and depends on input parameters given before performing the search, it has been written as a separate term.

The method of calculating the numerator and denominator are described in detail in [63] and [64], respectively. While the derivations are not repeated here, we wish to highlight that information about the population model is enfolded into the numerator; therefore, it is  $P(\vec{\theta} | \text{signal})$  that allows the pipeline to perform targeted source searches. The following section describes the changes made to improve the strongly-lensed gravitational-wave search.

### C. A better reduced template bank, and a lensing-based targeted population model

Traditional TESLA aims to reduce the noise background effectively to uncover possible strongly-lensed counterparts to the target super-threshold gravitational wave. We reduce the number of templates, and hence trials factors, by keeping only templates that can cover the parameter space where possible lensed counterparts may live in. Through an injection campaign, traditional TESLA locates a subset of templates from

the full template bank to construct a reduced template bank to search for possible lensed counterparts to a given target super-threshold gravitational wave. However, as explained at the beginning of IV, there are two problems in traditional TESLA, both of which lead to a decrease in the search sensitivity of TESLA.

We now propose two improvements to the TESLA method that will resolve these problems: (1) constructing a better reduced template bank, and (2) generating a targeted population model.

We recall that the sole purpose of the injection campaign is to determine the search parameter subspace that we should focus on to look for possible strongly-lensed sub-threshold counterparts to the target super-threshold gravitational waves. The injection campaign is always imperfect because we can only do a limited number of injections with discretized SNRs, i.e. we cannot cover the full spectrum of SNRs that possible lensed sub-threshold signals can have. Therefore, the templates that can recover lensed injections in the injection campaign can only serve as a pointer as to the region of search parameter space we should be targeting, i.e. a search parameter subspace where possible lensed sub-threshold counterparts to the target super-threshold gravitational waves may live in. We should hence use the injection campaign results to *define a boundary* within which templates live should be used collectively to construct the reduced template bank to search for possible lensed counterparts to the target, regardless of whether the templates can recover injections from the injection campaign. The proposed reduced template bank does not discard templates within the narrowed-down search parameter space defined by the boundary. Hence, it maintains the optimality guaranteed by the original full template bank within the limited search space. In turn, any possible lensed counterparts that live within the boundary will be recovered with an SNR loss less than 3%, preventing any loss of potential signals due to excessive SNR loss.

Under the strong lensing hypothesis, possible lensed counterparts should have the same parameters as the target super-threshold gravitational waves regardless of being super-threshold or sub-threshold. Therefore, the population of possible lensed counterparts to the target gravitational waves should have a higher probability of lying near the signal subspace defined by the posterior parameter probability distribution of the super-threshold event, and a lower probability of living far away from that. When we perform the injection campaign in traditional TESLA, we can obtain both the recovered injections' SNRs and the corresponding templates that recover the injections. Generally speaking, sub-threshold signals with lower optimal SNRs are affected by noise fluctuations more substantially and hence can be recovered by templates with parameters different from those of the target super-threshold event. That said, the templates closer to the signal subspace defined by the posterior parameter probability distribution of the target are associated with recovered injections with higher SNR values. Therefore, we can make use of the results from the injection campaign to construct a *Gaussian Kernel Density Estimation* (KDE) function  $\text{KDE}(\vec{\tau})$  using the distribution of the templates that recovered the lensed

injections, with the corresponding injections’ recovered SNRs as weights. The KDE is a function of source parameters  $\vec{\gamma}$ , which, to match the parameters of the template bank, are set to be the masses and spins of the source. When weighted with the recovered SNRs, regions closer to the signal subspace that the target super-threshold gravitational wave lies in will give a higher value for the KDE function, which matches our expectation that lensed counterparts to the target should have similar parameters as the target. The KDE function can then be redefined as the probability density function that describes the “source population” for our possible strongly-lensed sub-threshold counterparts to the target gravitational wave. Using this as our population model, we then follow the steps detailed in [63] to calculate  $P(\vec{\theta}|\text{signal})$ , i.e. the probability that a signal is recovered by a template with parameters  $\vec{\theta}$ . Notably, this probability depends on SNR, such that the search does not overly penalize templates far away from the signal subspace for weak sub-threshold signals. These methods instill a correct population model to the new TESLA method compared to the incorrect uniform population model in traditional TESLA, improving the search sensitivity.

#### D. The flow of the TESLA-X search method

We now describe in detail the actual flow of the proposed TESLA-X search method.

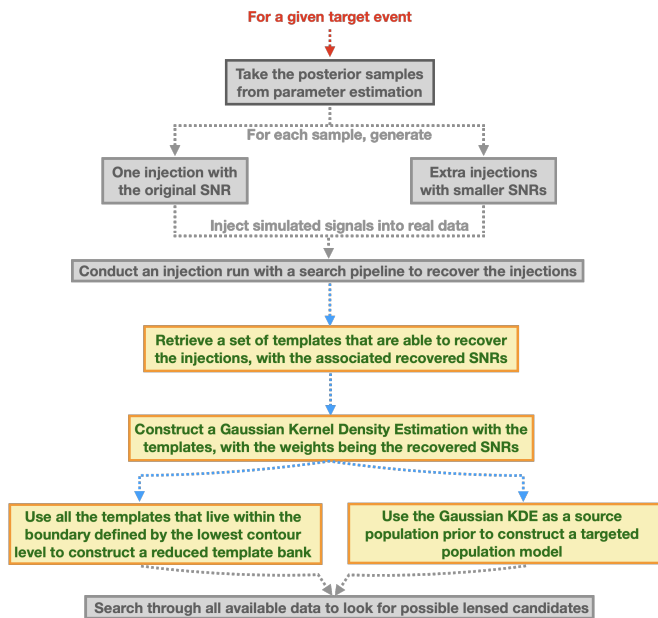


Figure 1. Workflow of TESLA-X. Elements in grey are the same procedures as in traditional TESLA. Colored elements (color online) are new procedures in TESLA-X.

Figure 1 presents the workflow of the TESLA-X method. We start with a target super-threshold gravitational-wave event found during a general search with GstLAL using a full template bank. Using the posterior samples obtained by Bayesian parameter estimation of the target event, we gener-

ate, for each sample, one injection that has the same optimal SNR as the sample, and nine additional injections with smaller optimal SNRs by increasing their effective distances, requiring that their SNRs in at least one detector have to be  $\geq 4$  to ensure they can be registered as a trigger during the matched-filtering process in the search. These injections will represent possible sub-threshold lensed counterparts to the target super-threshold event. We then inject these simulated lensed injections into real data, and use the GstLAL search pipeline to try and recover them with a full template bank. Up to this stage, TESLA-X is still identical to the traditional TESLA method.

After the injection campaign, we now retrieve a set of templates that can recover the simulated lensed injections, and the associated observed SNRs of the recovered injections. We can plot the retrieved templates on the chirp mass  $\mathcal{M}_c$  - effective spin  $\chi_{\text{eff}}$  space, with the colors of the points being the associated recovered injections’ observed SNRs  $\rho_{\text{obs}}$ . The top left panel of Figure 2 shows an example cartoon that plots the templates on the  $\mathcal{M}_c - \chi_{\text{eff}}$  space, with the color being the recovered injections’ network SNRs. Traditional TESLA keeps

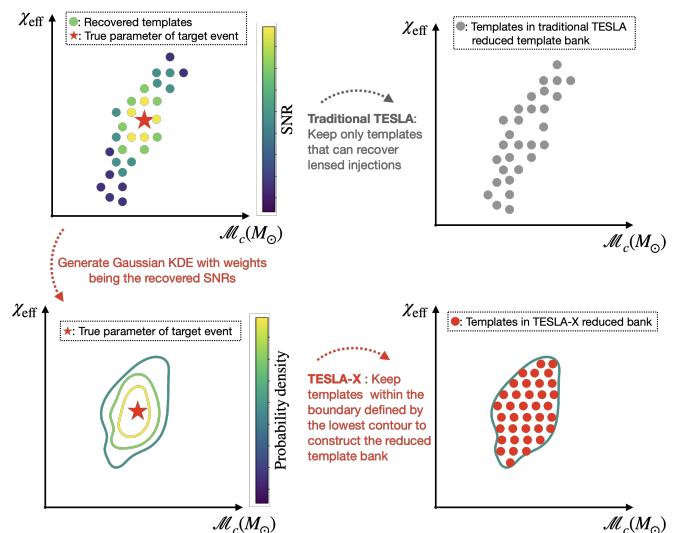


Figure 2. A cartoon depicting how we construct a reduced template bank from the injection results following the Traditional TESLA method (top right) and the proposed TESLA-X method (bottom left and right).

only templates that can recover the lensed injections and use them to construct the reduced bank, hereby known as “TESLA BANK” (top right panel of Figure 2). For TESLA-X, we construct a Gaussian Kernel Density Estimation (KDE) function  $f(\vec{\gamma})$  for the templates that recover the injections, with the corresponding recovered SNRs as the weights, where  $\vec{\gamma}$  is the set of template parameters we are considering; for example, in Figure 2  $\vec{\gamma}$  will be chirp mass  $\mathcal{M}_c$  and effective spin  $\chi_{\text{eff}}$ .

Note that the lensed injections are generated based on the posterior samples from the parameter estimation of the target event. Spins, admittedly, are not well measured for gravitational waves. However, recall that the lensed injections’ spin distribution follows the distribution of the parameter estimation result for the target event. Suppose the spin measurement

for the target event is poor. In that case, the parameter estimation result will essentially return the uninformed, uniform prior for spins, meaning that the lensed injections’ spins will follow a uniform distribution. Hence, the injection campaign result is not biased towards spins. Hence, we argue that there is no harm in using effective spin as a parameter when generating the Gaussian KDE.

Using the KDE function, we can then evaluate the probability density for each template point  $\vec{\theta}$  in the full template bank. We then use “matplotlib.pyplot.contour” with the default settings of “matplotlib.ticker.MaxNLocator” to determine the characteristic contour levels for the KDE function (see bottom left panel of Figure 2) for example). Then, using the lowest contour (it is left as future work to better define the lowest contour / least significant contour in terms of confidence interval) as the boundary, TESLA-X keeps *all* the templates within the boundary and uses them to construct the reduced template bank, hereby known as “TESLA-X BANK”. While the TESLA BANK has “holes” (see, for example, the top right picture in Figure 2) compared to the original full template bank because we are overly removing templates, the TESLA-X BANK keeps all the templates within a certain boundary, hence recovering the optimality of the original template bank in the region within the boundary. Hence, we will not lose signals due to excessive loss in SNR, and we will expect the TESLA-X BANK to give better search sensitivity.

Because the Gaussian KDE function  $f(\vec{\gamma})$  is essentially a probability density function (PDF) that describes the expected distribution of possible (sub-threshold) lensed counterparts to the target super-threshold gravitational wave, we can use it as the astrophysical source population prior to construct a targeted population model using the same methodology described in the previous section and [63]. Figure 3 shows an example cartoon to illustrate the idea. We have also compared

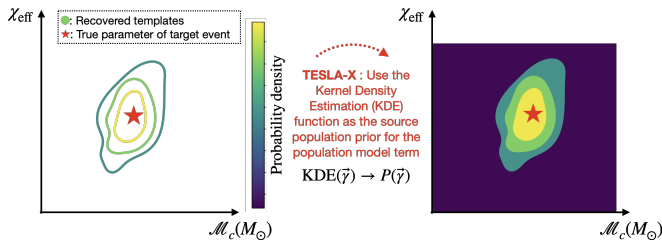


Figure 3. A cartoon depicting how we use the injection campaign results to construct a targeted population model in TESLA-X.

the performance of TESLA-X using (1) the targeted population model suggested above, and (2) an empirical, uniform mass model. We have verified that the search with the suggested targeted population model gives a better performance than the uniform mass model.

Once the reduced bank and the targeted population model have been constructed, we again use GstLAL to search through all possible data with the targeted bank and the targeted population model to look for potential sub-threshold lensed counterparts to the target super-threshold event. GstLAL will then output a list of candidate events ranked by their assigned ranking statistics, including the FARs and the likeli-

hood ratios  $\mathcal{L}$ . We have to stress again that the FARs assigned to the candidate events here do not quantify how likely they are to be lensed counterparts to the target event. Still, they are measures to distinguish noise triggers (false alarms) from real astrophysical signals, whether or not they are lensed counterparts to a target event. The ranking statistics here should only be used as a priority ranking for follow-up analysis to decide how likely each candidate event is a lensed counterpart to the target event. As future work, we will explore the idea of evaluating an additional lensing likelihood ratio for each trigger that includes additional lensing information as a separate ranking statistic. At that stage, the lensing likelihood may reveal how likely a trigger is a lensed counterpart to the target event.

## V. METHOD VERIFICATION AND RESULTS

In [44], we carry out a full-scale simulation campaign, where we prepare mock data with a pair of super-threshold and sub-threshold lensed signals injected, and apply the TESLA method to recover the two signals. We have proved that the TESLA method can recover sub-threshold lensed signals if they exist. TESLA-X and TESLA have essentially the same working principle, but the only differences are how we construct the reduced template bank and the population model. Therefore, we conduct a simulation campaign solely to compare the search effectiveness and sensitivity towards possible sub-threshold lensed gravitational-wave signals using TESLA and the proposed TESLA-X method.

### A. Mock data generation

First, we generate a 9.15-day long data stream with Gaussian noise recolored with O4 characteristic power spectral densities for LIGO Hanford, LIGO Livingston, and Virgo detector. The exact data for O4 characteristic power spectral densities for LIGO Hanford, LIGO Livingston and Virgo detector can be found at <https://dcc.ligo.org/T2200043-v3/public>. We assume that there is no detector downtime (Note: A detector is considered “down” if it is not in observing mode.), and no times are vetoed. We inject a super-threshold gravitational wave generated using the IMRPhenomXPHMpseudoFourPN waveform [65] into the mock data. Details about the source parameters of the injected gravitational wave are listed in Table I.

In later parts of this paper, we may refer to the super-threshold signal as MS220508a.

### B. Performing a general search

We then use GstLAL to perform a search over the mock data stream following the same settings used to search for gravitational waves within O3 data in GWTC-3 [66]. We use the same general template bank as described in [44] for the general search. As expected, the search recovers MS220508a with the highest ranking statistics (FAR=  $2.972 \times 10^{-35}$  Hz,

Properties	Injected super-threshold signal
UTC time	May 08 2022 11 : 06 : 00
GPS time	1336043178.397
Distance (Mpc)	2858.18
Primary mass $m_1^{\text{det}}$	$70.08 M_\odot$
Secondary mass $m_2^{\text{det}}$	$38.83 M_\odot$
Dimensionless spins	$\chi_{1x} = 0.182, \chi_{1y} = 0.182, \chi_{1z} = -0.0363,$ $\chi_{2x} = -0.113, \chi_{2y} = 0.132, \chi_{2z} = 0.116,$
Right ascension $\alpha$	2.811
Declination $\delta$	0.819
Inclination $\iota$	2.513
Polarization $\Psi$	1.187
Waveform	IMRPhenomXPHMpseudoFourPN

Table I. Information of the injected super-threshold gravitational-wave signal MS220508a in the simulation campaign. All properties reported here are measured in the detector frame.

rank 1) among all other triggers. We then apply a Bayesian inference library for gravitational-wave astronomy Bilby [60]<sup>1</sup> to perform parameter estimation (PE) for MS220508a, which outputs a set of posterior samples required to apply the TESLA and TESLA-X search pipeline.

### C. Performing an injection campaign

Using the posterior samples from the PE for MS220508a, we generated 7815 simulated lensed injections following equation 3. These simulated signals are injected into the mock data, and we perform another search using GstLAL with the general template bank to recover them. The results of the injection campaign are then used to perform the TESLA and TESLA-X analyses.

In the injection campaign, the general template bank recovers 6151 out of 7815 injections (See the column ‘‘General’’ in Table II), ringing up a total of 1008 templates (Note: The same template may be rung up multiple times by different injections, and hence the number of rung-up templates can be fewer than the number of found injections.). Figure 4 plots the rung-up templates on the chirp mass  $\mathcal{M}_c$  - effective spin  $\chi_{\text{eff}}$  space, with the colors of the markers being the network SNRs of the associated injections. We can see that the results match our expectations: Templates closer to the actual parameters of MS220508a are associated with injections with higher recovered SNRs (i.e. super-threshold). Those that have parameters much different than the actual parameters of MS220508a are, in general, related to injections with lower SNRs (i.e. sub-threshold).

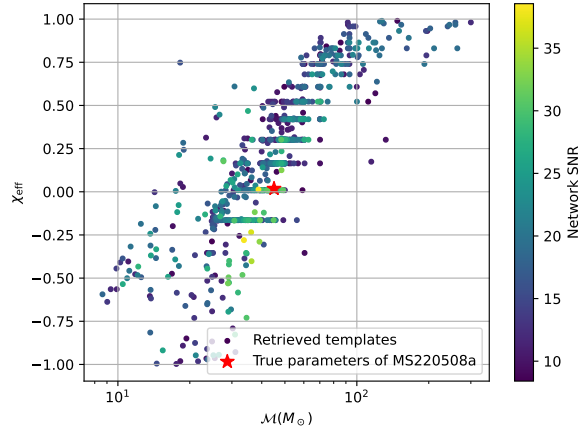


Figure 4. Rung-up templates by the simulated lensed injections of MS220508a in the injection campaign, plotted on the chirp mass  $\mathcal{M}_c$  - effective spin  $\chi_{\text{eff}}$  space. The colors of the markers represent the network SNRs of the associated injections.

### D. Generating the TESLA and TESLA-X reduced template banks

We keep all templates that are rung up during the injection campaign, and use them to generate a TESLA targeted template bank. Figure 5 shows the templates in the full template bank (in grey) and those in the TESLA template bank (in orange).

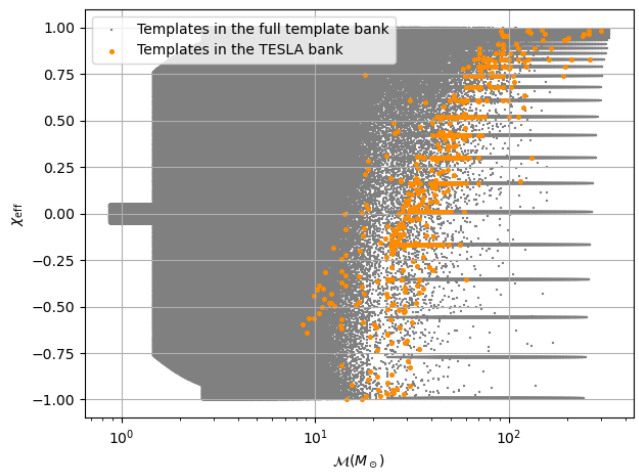


Figure 5. The templates in the full template bank (in grey) and in the TESLA reduced template bank (in orange), plotted in the  $\mathcal{M}_c$  -  $\chi_{\text{eff}}$  space.

For TESLA-X, we first use the rung-up templates in the injection campaign to construct a Gaussian Kernel Density Estimation (KDE) function  $\text{KDE}(\vec{\gamma})$  with the associated injections’ network SNRs as the weights.  $\gamma$  represents the template parameters used to label the templates. Here,  $\vec{\gamma} = \{\mathcal{M}_c, \chi_{\text{eff}}\}$ . Then, we evaluate the probability density at each template

<sup>1</sup> For reference, we used the default MCMC approach to do the sampling.

point in the full template bank, and plot the results on a contour map. Figure 6 shows the contour map for the Gaussian KDE function estimated for MS220508a.

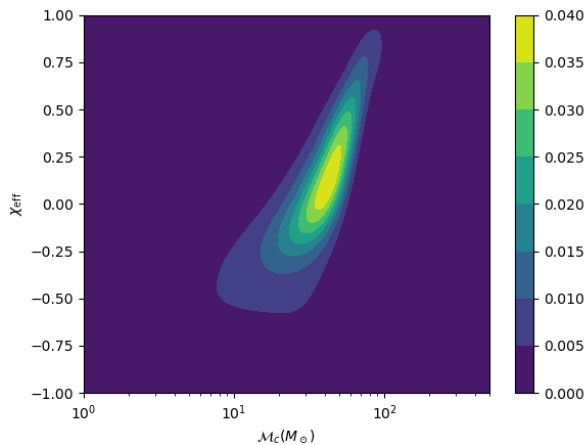


Figure 6. The contour map of the Gaussian Kernel Density Estimation function obtained for MS220508a in the  $\mathcal{M}_c - \chi_{\text{eff}}$  space. The colors represent the probability density estimated by the KDE function.

We then take the lowest contour level (For the case of MS220508a, the lowest contour level has a value of 0.005) as a boundary, and use all the templates within this boundary to construct a TESLA-X targeted template bank. Figure 7 shows the templates in the full template bank (in grey) and in the TESLA-X reduced template bank (in red) in the  $\mathcal{M}_c - \chi_{\text{eff}}$  space. The yellow curve marks the lowest contour level we obtained for the estimated Gaussian KDE function we showed in Figure 6. There are 22136 templates in the TESLA-X reduced template bank.

### E. Constructing the targeted population model for the TESLA-X reduced template bank

Next, we use the estimated KDE function for MS220508a and the TESLA-X reduced template bank to construct a targeted population model, following the same steps detailed in IV and [63]. Note that for practical reasons, the Gaussian KDE function  $\text{KDE}(\vec{\gamma})$  is re-calculated with  $\vec{\gamma}$  chosen to be the component masses and spins  $m_1, m_2, \chi_1, \chi_2$  instead of  $\mathcal{M}_c$  and  $\chi_{\text{eff}}$ .

### F. Performing a re-filtering to recover the lensed injections with the TESLA and TESLA-X methods

Finally, we perform two searches, one using the TESLA reduced template bank, and one using the TESLA-X reduced template bank, together with the targeted population model, over the same stretch of mock data to try to recover the same set of lensed injections used in the injection campaign to com-

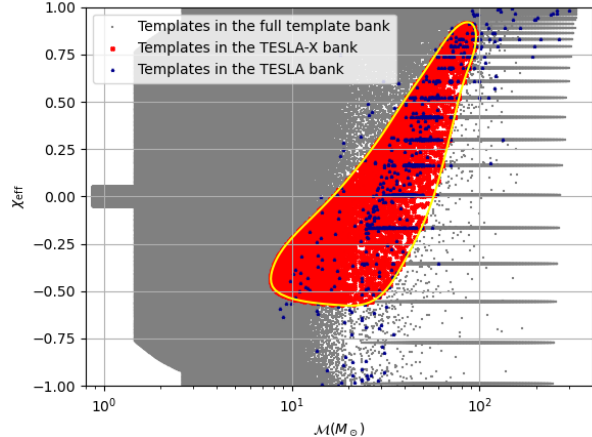


Figure 7. The templates in the full template bank (in grey) and in the TESLA-X reduced template bank (in red), plotted in the  $\mathcal{M}_c - \chi_{\text{eff}}$  space. The TESLA-X template bank is constructed by keeping templates that fall within the lowest contour level from the Gaussian KDE function shown in Figure 6, i.e. 0.005, plotted as a yellow curve in this figure. For easy comparison, we plot the TESLA reduced template bank templates in the same figure (in blue).

pare the performance of the TESLA and TESLA-X methods. Table II summarizes the findings. As expected, the TESLA method successfully recovers more injections than the full template bank, with an increase of 0.29%. However, we can see that the proposed TESLA-X method outperforms the TESLA method. In particular, it recovers even more lensed injections than the TESLA method, with an increase of 2.37%.

Injections	General	TESLA	TESLA-X
Total	7815	7815	7815
Found	6151	6169	6297
Found % change	-	+0.29%	+2.37%

Table II. Number of injections found during the search of mock data using the general template bank, TESLA method, and TESLA-X method, respectively.

Furthermore, if we look at the sensitive range v.s. FAR for MS220508a-alike signals using the full template bank, TESLA template bank, and TESLA-X template bank, respectively (see Figure 8), we can see that the TESLA-X method gives a bigger improvement in terms of sensitivity towards MS220508a-alike (lensed) signals than the traditional TESLA method. In particular, we note that the improvement is most significant in the region with  $\text{FAR} \geq 10^{-7}$  Hz, which represents the “sub-threshold” region. This means that TESLA-X outperforms TESLA in finding possible sub-threshold strongly lensed gravitational waves.

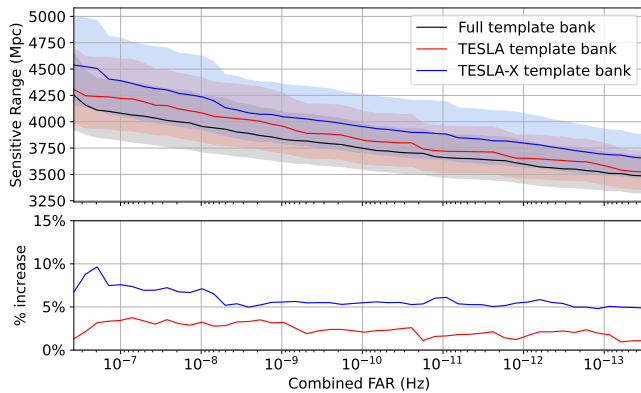


Figure 8. (Top panel) The sensitive range v.s. FAR for MS220508a-like signals using the full template bank (black), TESLA template bank (red), and TESLA-X template bank (blue), respectively. The shaded band for each curve represents the corresponding 1-sigma region. (Bottom panel) The corresponding percentage changes in sensitive range v.s. FAR for the different banks. We note that both the TESLA and TESLA-X bank improves in terms of sensitivity towards MS220508a-like (lensed) signals, but the curve representing the TESLA-X bank (blue) is above that of the TESLA bank (red), meaning that the TESLA-X method outperforms the TESLA method. In particular, notice that the improvement is most significant in the region with  $\text{FAR} \geq 10^{-7}$  Hz, which represents the “sub-threshold” region. This further proves that the TESLA-X method is better than the traditional TESLA method.

## VI. CONCLUDING REMARKS

The detectability of strongly lensed gravitational wave (GW) signals can be compromised as they may experience demagnification, falling below the detection threshold. In a previous study, we introduced the TESLA method [44] to extract strongly lensed sub-threshold GW signals by constructing a target template bank based on the information from detected events. This paper presents an enhanced approach called TESLA-X, which aims to improve the search sensitivity for strongly lensed sub-threshold GW signals.

The TESLA-X methodology begins with generating simulated lensed injections using posterior samples obtained from parameter estimation. These injections are then subjected to an injection campaign using GstLAL, with a threshold set at a FAR of  $3.385 \times 10^{-7}$  Hz, ensuring statistical significance. Subsequently, the TESLA-X method utilizes the retrieved injections to create a targeted population model and a densely distributed template bank. Finally, the data is reprocessed to identify potential sub-threshold lensed candidates using the new population model and template bank.

The targeted population model is constructed through several steps. Initially, a Gaussian kernel density estimation (KDE) function is applied to the retrieved injections’ source parameters  $\vec{\gamma}$ . This KDE function is then transformed into a probability density function, representing the parameter space of our potential strong-lensed sub-threshold GW signals [63]. Additionally, we generate the targeted template bank by defining a boundary within the retrieved injections. This process

involves discarding templates from the original full template bank outside of a predefined boundary that encloses the target parameter space while keeping all templates within the boundary. This results in a densely distributed template bank targeting a smaller region. Compared to the TESLA method, this refined template bank ensures the recovery of any lensed counterparts with less than a 3% SNR loss. Notably, the FARs and likelihood values ( $\mathcal{L}$ ) do not provide information about the likelihood of being lensed counterparts to the target event. Instead, they serve as metrics to differentiate between noise triggers and astrophysical signals.

In this study, we conducted a simulation campaign to evaluate and compare the search sensitivity of three methods: the full template bank search, the TESLA method, and the TESLA-X method. Our analysis utilized a stream of mock data, where Gaussian noise was introduced along with a significant GW event labeled MS220508a. Our findings demonstrate that the TESLA-X method outperforms the other approaches by successfully recovering more lensed injections specifically targeting MS220508a. Furthermore, we observed a maximum of  $\sim 10\%$  increase in the search sensitivity through an examination of the sensitive range versus FAR plot. An increase in sensitive range means that we can see signals coming from further sources, and equivalently, we can see weaker signals according to equation 3. These results substantiate the superior performance of the TESLA-X method in enhancing the search capabilities for gravitational lensing phenomena. TESLA-X still carries the same problem as TESLA in terms of high computational cost (For reference, running TESLA/TESLA-X for a single super-threshold event can take  $\mathcal{O}(\text{weeks})$ .) for running the injection campaign for each target super-threshold gravitational-wave event. As future work, we will explore ways to improve TESLA-X’s computational efficiency. We will also look into possible parameters other than chirp mass and effective spin to represent our interested population (See Appendix).

## ACKNOWLEDGMENTS

The authors acknowledge the generous support from the National Science Foundation in the United States. AKYL would like to gratefully acknowledge the support from the National Science Foundation through the Grants NSF PHY-1912594 and NSF PHY-2207758. JCLC acknowledges support from the Villum Investigator program supported by the VILLUM Foundation (grant no. VIL37766) and the DNRF Chair program (grant no. DNRF162) by the Danish National Research Foundation. HF gratefully acknowledges the support of the Canadian Institute for Theoretical Astrophysics (CITA) National Fellowship and the Japan Society for the Promotion of Science (JSPS) Postdoctoral Fellowships for Research in Japan. JME is supported by the European Union’s Horizon 2020 research and innovation program under the Marie Skłodowska-Curie grant agreement No. 847523 INTERACTIONS, and by VILLUM FONDEN (grant no. 53101 and 37766).

The authors are also grateful for computational resources

provided by the LIGO Laboratory and supported by National Science Foundation Grants PHY-0757058 and PHY-0823459. This research has made use of data, software and/or web tools obtained from the Gravitational Wave Open Science Center (<https://www.gw-openscience.org>) [67], a service of LIGO Laboratory, the LIGO Scientific Collaboration and the Virgo Collaboration. LIGO was constructed by the California Institute of Technology and Massachusetts Institute of Technology with funding from the National Science Foundation and operates under cooperative agreement PHY-0757058. HF is supported by a CITA National Fellowship. Virgo is funded by the French Centre National de Recherche Scientifique (CNRS), the Italian Istituto Nazionale della Fisica Nucleare (INFN) and the Dutch Nikhef, with contributions by Polish and Hungarian institutes. This paper carries LIGO Document Number LIGO-P1900059.

### Appendix A: Choosing a suitable pair of parameters to construct the Gaussian KDE

In the main text, we construct the Gaussian KDE in the chirp mass  $\mathcal{M}_c$  - effective spin  $\chi_{\text{eff}}$  parameter space. It has also been suggested that the component masses  $m_1$ - $m_2$  parameter space may be a better choice. In this appendix, we present some preliminary investigation results for this question.

#### 1. Re-doing the TESLA-X analysis for MS220508a with the Gaussian KDE constructed in the $m_1$ - $m_2$ space

In this subsection, we redo the TESLA-X analysis with the Gaussian KDE constructed in the component masses  $m_1$ - $m_2$  parameter space instead of the chirp mass  $\mathcal{M}_c$  - effective spin  $\chi_{\text{eff}}$  parameter space.

##### a. Constructing the TESLA-X bank and population model

We start with the injection run results we obtained previously for the same event. First, Figure 9 plots the rung-up templates on the component masses  $m_1$ - $m_2$  parameter space, with the colors of the markers being the network SNRs of the associated injections.

Note that although we are working in a different parameter space, templates in the TESLA template bank will remain unchanged because we are simply keeping all the templates that are rung up by the injections during the injection campaign to form the TESLA bank. For completeness, we also plot the **same** TESLA bank in the main text for MS220508a on the component masses  $m_1$ - $m_2$  parameter space in Figure 10. As before, templates in the full template bank are plotted in grey, and those in the TESLA template bank are plotted in orange.

For TESLA-X, we use the rung-up templates in the injection campaign to construct a Gaussian Kernel Density Estimation (KDE) function  $\text{KDE}(\vec{\gamma})$  with the associated injections' network SNRs as the weights. As before,  $\gamma$  represents

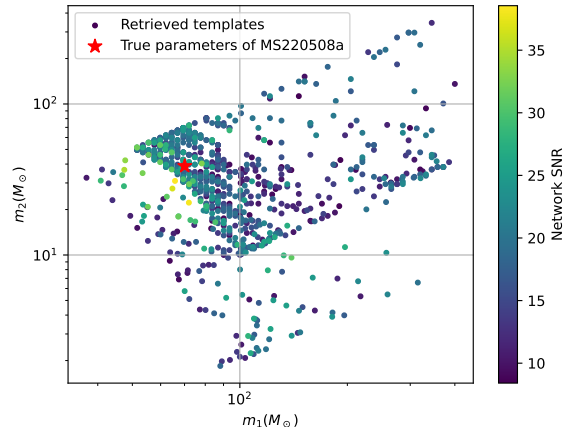


Figure 9. Rung-up templates by the simulated lensed injections of MS220508a in the injection campaign, plotted on the component masses  $m_1$ - $m_2$  parameter space. The colors of the markers represent the network SNRs of the associated injections.

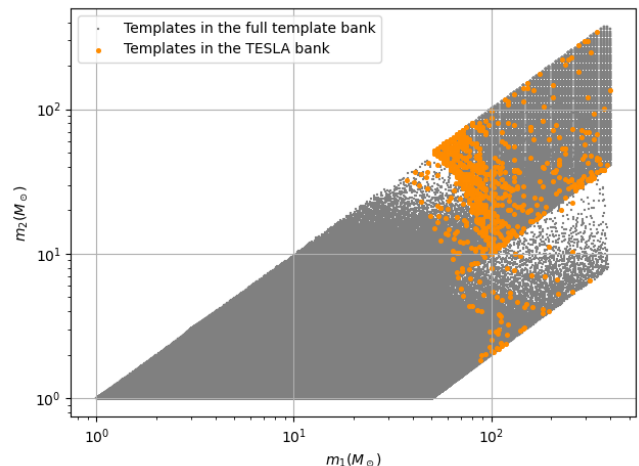


Figure 10. The templates in the full template bank (in grey) and in the TESLA reduced template bank (in orange), plotted in the component masses  $m_1$ - $m_2$  space.

the template parameters used to label the templates. Here,  $\vec{\gamma} = \{m_1, m_2\}$ . Then, we evaluate the probability density at each template point in the full template bank, and plot the results on a contour map. Figure 11 shows the contour map for the Gaussian KDE function estimated for MS220508a in the  $m_1$ - $m_2$  space.

We again take the lowest contour level (0.00002) as a boundary, and use all the templates that fall within this boundary to construct a TESLA-X targeted template bank in the  $m_1$ - $m_2$  space. For simplicity, we will call the TESLA-X bank created based on the KDE constructed in the  $m_1$ - $m_2$  space as the “TESLA-X (component mass) bank”, and the TESLA-X bank in the main text that is created based on the KDE constructed in the  $\mathcal{M}_c$  -  $\chi_{\text{eff}}$  space as the “TESLA-X (main) bank”. Fig-

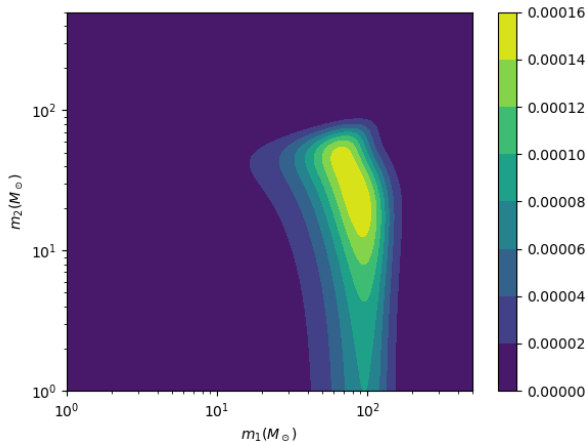


Figure 11. The contour map of the Gaussian Kernel Density Estimation function obtained for MS220508a in the  $m_1 - m_2$  space. The colors represent the probability density estimated by the KDE function.

Figure 12 shows the templates in the full template bank (in grey) and in the “TESLA-X (component mass) bank” (in red) in the  $m_1 - m_2$  space. The yellow curve marks the lowest contour level we obtained for the estimated Gaussian KDE function we showed in Figure 11. There are 159043 templates in the “TESLA-X (component mass) bank”.

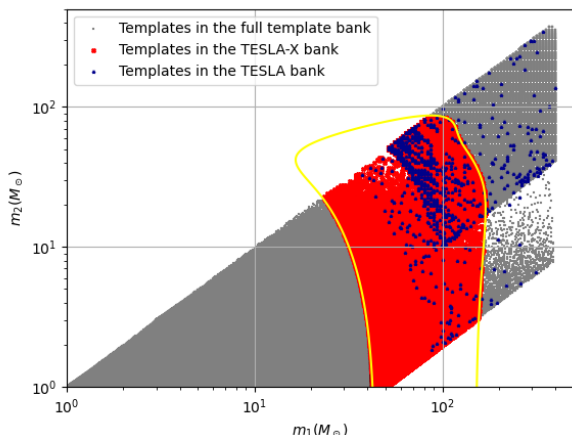


Figure 12. The templates in the full template bank (in grey) and in the “TESLA-X (component mass) bank” (in red), plotted in the  $m_1 - m_2$  space. The “TESLA-X (component mass) bank” is constructed by keeping templates that fall within the lowest contour level from the Gaussian KDE function shown in Figure 11, i.e. 0.00002, plotted as a yellow curve in this figure. For easy comparison, we also plot the templates in the TESLA reduced template bank in the same figure (in blue).

Similar to the main text, we use the estimated KDE function for MS220508a and the “TESLA-X (component mass) bank” to construct a targeted population model, following the same

steps detailed in IV and [63].

- b. *Trying to recover the lensed injections with the “TESLA-X (main) bank” and “TESLA-X (component mass) bank”*

To compare the effectiveness of the “TESLA-X (main) bank” and “TESLA-X (component mass) bank” for the case of MS220508a, we perform an additional search using the “TESLA-X (component mass) bank” together with the targeted population model over the same stretch of mock data described in the main text to try to recover the same set of lensed injections used in the injection campaign. Table III summarizes the findings. We can see that “TESLA-X (component mass)” is performing even worse than the full template bank, with a reduction in recovered lensed injections by  $-0.3\%$ . This should not be surprising, however, given that the “TESLA-X (component mass) bank” has more templates than the “TESLA-X (main) bank” (almost six times more templates). This results in a much higher trials factor and, hence, a larger noise background, making it harder to recover the simulated lensed injections.

Injections	General	TESLA-X (main)	TESLA-X (component mass)
Total	7815	7815	7815
Found	6151	6297	6132
Found % change	-	+2.37%	-0.3%

Table III. Number of injections found during the search of mock data using the general template bank, “TESLA-X (main) bank” and “TESLA-X (component mass) bank” respectively.

Furthermore, if we look at the sensitive range v.s. FAR for MS220508a-alike signals using the full template bank, “TESLA-X (main) bank” and “TESLA-X (component mass) bank” respectively (see Figure 13), we can see that the “TESLA-X (component mass) bank” is performing even worse than the full template bank. Therefore, in the case of MS220508a, chirp mass  $\mathcal{M}_c$  - effective spin  $\chi_{\text{eff}}$  would be the better pair of parameters to construct the Gaussian KDE in the TESLA-X method.

## 2. Analyzing another mock event MS220510ae with the TESLA-X method

MS220508a is a relatively low chirp mass event ( $\sim 45.0 M_\odot$ ). It will be useful to redo the above investigation about the choice of parameters to construct the Gaussian KDE in the TESLA-X method with a different mock event that lives in a different region in the parameter space.

In this subsection, we repeat the analysis in the previous subsection with another mock superthreshold gravitational-wave event MS220510ae. Settings for the mock data are identical to those in the main text. Details about the source parameters of the injected gravitational wave are listed in Table IV.

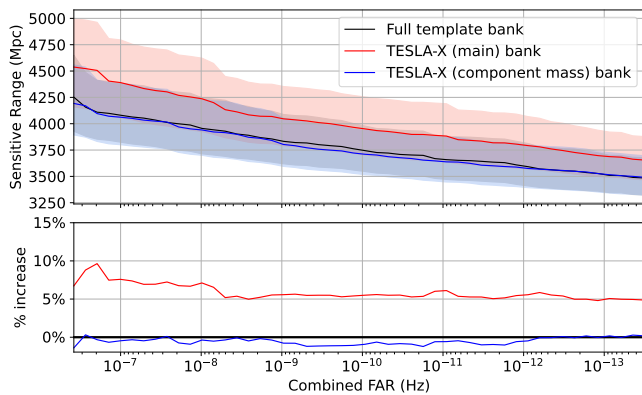


Figure 13. (Top panel) The sensitive range v.s. FAR for MS220508a-like signals using the full template bank (black), “TESLA-X (main) bank” (red), and “TESLA-X (component mass) bank” (blue) respectively. The shaded band for each curve represents the corresponding 1-sigma region. (Bottom panel) The corresponding percentage changes in sensitive range v.s. FAR for the different banks. We note that while the “TESLA-X (main) bank” improves in terms of sensitivity towards MS220508a-like (lensed) signals, “TESLA-X (component mass) bank” is performing worse than the full template bank, mainly due to the significant increase in trials factors caused by the large number of templates.

Properties	Injected super-threshold signal
UTC time	May 10 2022 18 : 38 : 17
GPS time	1336243115.828
Distance (Mpc)	10066.811
Primary mass $m_1^{\text{det}}$	$166.90M_{\odot}$
Secondary mass $m_2^{\text{det}}$	$117.04M_{\odot}$
Dimensionless spins	$\chi_{1x} = 0.635, \chi_{1y} = 0.233, \chi_{1z} = 0.660,$ $\chi_{2x} = 0.006, \chi_{2y} = 0.087, \chi_{2z} = 0.029,$
Right ascension $\alpha$	5.69
Declination $\delta$	1.45
Inclination $\iota$	5.99
Polarization $\Psi$	2.92
Waveform	IMRPhenomXPHMpseudoFourPN

Table IV. Information of the injected super-threshold gravitational-wave signal MS220510ae in the simulation campaign. All properties reported here are measured in the detector frame.

We follow the same steps in the main text to perform Bayesian parameter estimation on MS220510ae, and use the posterior samples obtained to generate a set of lensed injections. We then conduct an injection campaign using the full template bank to search for the lensed injections. The injection run results are then used to construct the “TESLA-X (main) bank” and “TESLA-X (component mass) bank”, and their corresponding targeted population models. Out of the 8099 lensed injections, the full template bank manages to recover 5047. For simplicity, we only show the Gaussian KDE constructed for the “TESLA-X (main) bank” (in the  $\mathcal{M}_c - \chi_{\text{eff}}$  space) and for the “TESLA-X (component mass) bank” (in the  $m_1 - m_2$  space) in Figure 14 and 15 respectively.

As before, we construct the “TESLA-X (main) bank” and

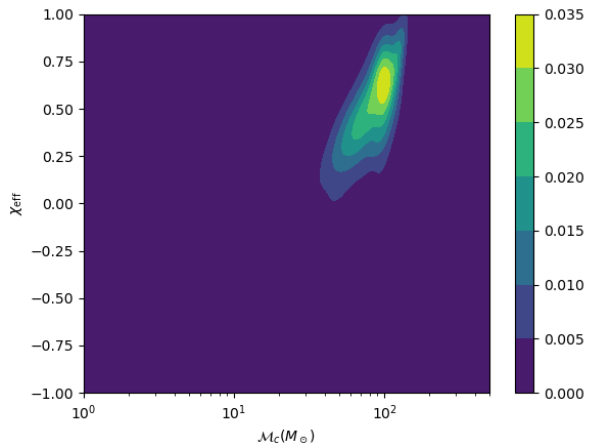


Figure 14. The contour map of the Gaussian Kernel Density Estimation function obtained for MS220510ae in the  $\mathcal{M}_c - \chi_{\text{eff}}$  space. The colors represent the probability density estimated by the KDE function.

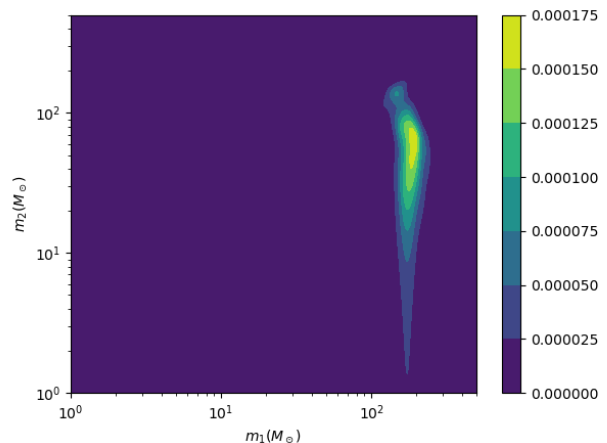


Figure 15. The contour map of the Gaussian Kernel Density Estimation function obtained for MS220510ae in the  $m_1 - m_2$  space. The colors represent the probability density estimated by the KDE function.

“TESLA-X (component mass) bank” by keeping all templates that fall within the boundary defined by the least significant contour in the respective Gaussian KDE constructed. For the case of MS220510ae, the “TESLA-X (main) bank” contains 15655 templates, and the “TESLA-X (component mass) bank” contains 21676 templates. Notice that the “TESLA-X (component mass) bank” for MS220510ae, unlike in the case for MS220508a, is larger than the “TESLA-X (main) bank” by merely  $\sim 5000$  templates.

We then use the two TESLA-X banks and their respective population models to try recovering the same set of lensed injections used in the injection campaign. Table V summarizes the findings. Completely different from the case of MS220508a in the main text, we can see that “TESLA-X

(component mass)” is performing even better than the full template bank, while the “TESLA-X (main) bank” is performing worse than the full template bank. This is mainly because spins are poorly measured in general for high-mass systems, and hence the “TESLA-X (main) bank”, with inaccurate constraint in the spin dimension, are more likely to lose signals than the “TESLA-X (component mass) bank”, which does not impose any constraints on spins. For completeness, we also show the sensitive range v.s. FAR for MS220510ae-like signals using the full template bank, “TESLA-X (main) bank” and “TESLA-X (component mass) bank” respectively in Figure 16.

Injections	General	TESLA-X (main)	TESLA-X (component mass)
Total	8099	8099	8099
Found	5047	4715	5886
Found % change	-	-6.58%	16.6%

Table V. Number of injections found during the search of mock data using the general template bank, “TESLA-X (main) bank” and “TESLA-X (component mass) bank” respectively for the mock event MS220510ae.

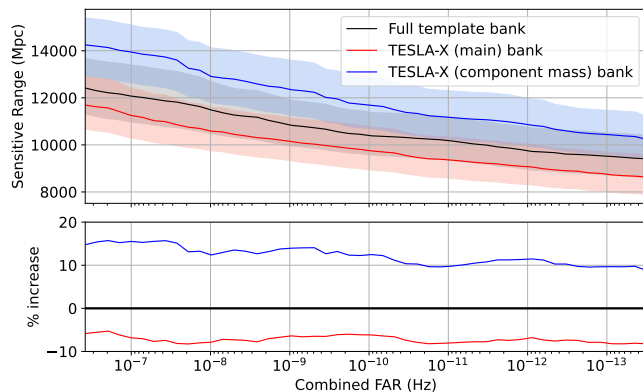


Figure 16. (Top panel) The sensitive range v.s. FAR for MS220510ae-like signals using the full template bank (black), “TESLA-X (main) bank” (red), and “TESLA-X (component mass) bank” (blue) respectively. The shaded band for each curve represents the corresponding 1-sigma region. (Bottom panel) The corresponding percentage changes in sensitive range v.s. FAR for the different banks. We note that, unlike the case of MS220508a in the main text, the “TESLA-X (component mass) bank” improves in terms of sensitivity towards MS220510ae-like (lensed) signals, “TESLA-X (main) bank” performs worse than the full template bank. This is mainly because spins are typically poorly measured for high chirp mass systems.

### 3. Conclusion

From the two investigations, we note that “chirp mass - effective spins” is a better parameter pair to be used in constructing the Gaussian KDE for the TESLA-X method, if the

target event is a low chirp mass system. On the other hand, component masses “mass 1 - mass 2” will be a better parameter pair to be used in constructing the Gaussian KDE for the TESLA-X method, if the target event is a high chirp mass system. We note that these findings are entirely expected: While chirp masses and spins are well-measured in low-mass systems, they are not well-measured in high-mass systems since their signals have much fewer in-band cycles. As future work, we will investigate how we can improve the construction of the Gaussian KDE functions for the TESLA-X method. For instance, we can see that the Gaussian KDEs can exceed the physical boundary of the original template bank (See the yellow boundary in 12). Regions near the physical boundary of the original template bank may require special care. We may also explore the idea of first constructing and applying a separate KDE to “flatten” the TESLA-X bank (i.e., to construct a uniform mass model) before applying the Gaussian KDE representing the targeted population model.

- [1] H. Ohanian, *Int. J. Theor. Phys.* **9**, 425 (1974).
- [2] K. Thorne, in *Les Houches Summer School on Gravitational Radiation* (1982) pp. 1–57.
- [3] S. Deguchi and W. D. Watson, *Phys. Rev. D* **34**, 1708 (1986).
- [4] Y. Wang, A. Stebbins, and E. L. Turner, *Phys. Rev. Lett.* **77**, 2875 (1996), arXiv:astro-ph/9605140.
- [5] T. T. Nakamura, *Phys. Rev. Lett.* **80**, 1138 (1998).
- [6] R. Takahashi and T. Nakamura, *Astrophys. J.* **595**, 1039 (2003), arXiv:astro-ph/0305055.
- [7] L. Dai and T. Venumadhav, arXiv e-prints, arXiv:1702.04724 (2017), arXiv:1702.04724 [gr-qc].
- [8] J. M. Ezquiaga, D. E. Holz, W. Hu, M. Lagos, and R. M. Wald, *Phys. Rev. D* **103**, 6 (2021), arXiv:2008.12814 [gr-qc].
- [9] K. K. Ng, K. W. Wong, T. Broadhurst, and T. G. Li, *Phys. Rev. D* **97**, 023012 (2018), arXiv:1703.06319 [astro-ph.CO].
- [10] S.-S. Li, S. Mao, Y. Zhao, and Y. Lu, *Mon. Not. Roy. Astron. Soc.* **476**, 2220 (2018), arXiv:1802.05089 [astro-ph.CO].
- [11] M. Oguri, *Mon. Not. Roy. Astron. Soc.* **480**, 3842 (2018), arXiv:1807.02584 [astro-ph.CO].
- [12] G. P. Smith, M. Jauzac, J. Veitch, W. M. Farr, R. Massey, and J. Richard, *Mon. Not. Roy. Astron. Soc.* **475**, 3823 (2018), arXiv:1707.03412 [astro-ph.HE].
- [13] G. Smith *et al.*, *IAU Symp.* **338**, 98 (2017), arXiv:1803.07851 [astro-ph.CO].
- [14] G. P. Smith, A. Robertson, M. Bianconi, and M. Jauzac, arXiv e-prints, arXiv:1902.05140 (2019), arXiv:1902.05140 [astro-ph.HE].
- [15] A. Robertson, G. P. Smith, R. Massey, V. Eke, M. Jauzac, M. Bianconi, and D. Ryczanowski, *Mon. Not. Roy. Astron. Soc.* **495**, 3727 (2020), arXiv:2002.01479 [astro-ph.CO].
- [16] D. Ryczanowski, G. P. Smith, M. Bianconi, R. Massey, A. Robertson, and M. Jauzac, *Mon. Not. Roy. Astron. Soc.* **495**, 1666 (2020), arXiv:2005.02296 [astro-ph.GA].
- [17] J. M. Ezquiaga, W. Hu, and R. K. L. Lo, *Phys. Rev. D* **108**, 103520 (2023), arXiv:2308.06616 [astro-ph.CO].
- [18] Z. Cao, L.-F. Li, and Y. Wang, *Phys. Rev. D* **90**, 062003 (2014).
- [19] K.-H. Lai, O. A. Hannuksela, A. Herrera-Martín, J. M. Diego, T. Broadhurst, and T. G. Li, *Phys. Rev. D* **98**, 083005 (2018), arXiv:1801.07840 [gr-qc].
- [20] P. Christian, S. Vitale, and A. Loeb, *Phys. Rev. D* **98**, 103022 (2018), arXiv:1802.02586 [astro-ph.HE].
- [21] L. Dai, S.-S. Li, B. Zackay, S. Mao, and Y. Lu, *Phys. Rev. D* **98**, 104029 (2018), arXiv:1810.00003 [gr-qc].
- [22] J. Diego, O. Hannuksela, P. Kelly, T. Broadhurst, K. Kim, T. Li, G. Smoot, and G. Pagano, *Astron. Astrophys.* **627**, A130 (2019), arXiv:1903.04513 [astro-ph.CO].
- [23] M. Çalişkan, L. Ji, R. Cotesta, E. Berti, M. Kamionkowski, and S. Marsat, *Phys. Rev. D* **107**, 043029 (2023), arXiv:2206.02803 [astro-ph.CO].
- [24] M. H. Y. Cheung, J. Gais, O. A. Hannuksela, and T. G. F. Li, *Mon. Not. Roy. Astron. Soc.* **503**, 3326 (2021), arXiv:2012.07800 [astro-ph.HE].
- [25] A. Mishra, A. K. Meena, A. More, S. Bose, and J. S. Bagla, arXiv e-prints, arXiv:2102.03946 (2021), arXiv:2102.03946 [astro-ph.CO].
- [26] A. K. Meena, A. Mishra, A. More, S. Bose, and J. S. Bagla, *Mon. Not. Roy. Astron. Soc.* **517**, 872 (2022), arXiv:2205.05409 [astro-ph.GA].
- [27] P. Cremonese, J. M. Ezquiaga, and V. Salzano, *Phys. Rev. D* **104**, 023503 (2021), arXiv:2104.07055 [astro-ph.CO].
- [28] M. Çalişkan, N. Anil Kumar, L. Ji, J. M. Ezquiaga, R. Cotesta, E. Berti, and M. Kamionkowski, *Phys. Rev. D* **108**, 123543 (2023), arXiv:2307.06990 [astro-ph.CO].
- [29] J. M. Ezquiaga and M. Zumalacárregui, *Phys. Rev. D* **102**, 124048 (2020), arXiv:2009.12187 [gr-qc].
- [30] T. Baker and M. Trodden, *Phys. Rev. D* **95**, 063512 (2017), arXiv:1612.02004 [astro-ph.CO].
- [31] T. E. Collett and D. Bacon, *Phys. Rev. Lett.* **118**, 091101 (2017), arXiv:1602.05882 [astro-ph.HE].
- [32] S. Goyal, A. Vijaykumar, J. M. Ezquiaga, and M. Zumalacárregui, *Phys. Rev. D* **108**, 024052 (2023), arXiv:2301.04826 [gr-qc].
- [33] O. A. Hannuksela, T. E. Collett, M. Çalişkan, and T. G. F. Li, *Mon. Not. Roy. Astron. Soc.* **498**, 3395 (2020), arXiv:2004.13811 [astro-ph.HE].
- [34] H. Yu, P. Zhang, and F.-Y. Wang, *Mon. Not. Roy. Astron. Soc.* **497**, 204 (2020), arXiv:2007.00828 [astro-ph.CO].
- [35] M. Oguri and R. Takahashi, *Astrophys. J.* **901**, 58 (2020), arXiv:2007.01936 [astro-ph.CO].
- [36] A. Liu, I. C. F. Wong, S. H. W. Leong, A. More, O. A. Hannuksela, and T. G. F. Li, *Mon. Not. Roy. Astron. Soc.* **525**, 4149 (2023), arXiv:2302.09870 [gr-qc].
- [37] M. Sereno, P. Jetzer, A. Sesana, and M. Volonteri, *Mon. Not. Roy. Astron. Soc.* **415**, 2773 (2011), arXiv:1104.1977 [astro-ph.CO].
- [38] K. Liao, X.-L. Fan, X.-H. Ding, M. Biesiada, and Z.-H. Zhu, *Nature Commun.* **8**, 1148 (2017), [Erratum: *Nature Commun.* **8**, 2136 (2017)], arXiv:1703.04151 [astro-ph.CO].
- [39] S. Cao, J. Qi, Z. Cao, M. Biesiada, J. Li, Y. Pan, and Z.-H. Zhu, *Sci. Rep.* **9**, 11608 (2019), arXiv:1910.10365 [astro-ph.CO].
- [40] F. Xu, J. M. Ezquiaga, and D. E. Holz, *Astrophys. J.* **929**, 9 (2022), arXiv:2105.14390 [astro-ph.CO].
- [41] O. A. Hannuksela, K. Haris, K. K. Y. Ng, S. Kumar, A. K. Mehta, D. Keitel, T. G. F. Li, and P. Ajith, *Astrophys. J. Lett.* **874**, L2 (2019), arXiv:1901.02674 [gr-qc].
- [42] R. Abbott *et al.* (LIGO Scientific, VIRGO), *Astrophys. J.* **923**, 14 (2021), arXiv:2105.06384 [gr-qc].
- [43] R. Abbott *et al.* (LIGO Scientific, VIRGO, KAGRA), arXiv e-prints, arXiv:2304.08393 (2023), arXiv:2304.08393 [gr-qc].
- [44] A. K. Y. Li, R. K. L. Lo, S. Sachdev, J. C. L. Chan, E. T. Lin, T. G. F. Li, and A. J. Weinstein (LIGO Scientific, Virgo), *Phys. Rev. D* **107**, 123014 (2023), arXiv:1904.06020 [gr-qc].
- [45] C. McIsaac, D. Keitel, T. Collett, I. Harry, S. Mozzon, O. Edy, and D. Bacon, *Phys. Rev. D* **102**, 084031 (2020), arXiv:1912.05389 [gr-qc].
- [46] L. Dai, B. Zackay, T. Venumadhav, J. Roulet, and M. Zaldarriaga, arXiv e-prints, arXiv:2007.12709 (2020), arXiv:2007.12709 [astro-ph.HE].
- [47] X. Liu, I. M. Hernandez, and J. Creighton, *Astrophys. J.* **908**, 97 (2021), arXiv:2009.06539 [astro-ph.HE].
- [48] A. R. A. C. Wierda, E. Wempe, O. A. Hannuksela, L. e. V. E. Koopmans, and C. Van Den Broeck, *Astrophys. J.* **921**, 154 (2021), arXiv:2106.06303 [astro-ph.HE].
- [49] B. P. Abbott *et al.* (KAGRA, LIGO Scientific, Virgo, VIRGO), *Living Rev. Rel.* **21**, 3 (2018), arXiv:1304.0670 [gr-qc].
- [50] C. Messick *et al.*, *Phys. Rev. D* **95**, 042001 (2017), arXiv:1604.04324 [astro-ph.IM].
- [51] S. Sachdev *et al.*, (2019), arXiv:1901.08580 [gr-qc].
- [52] C. Hanna *et al.*, *Phys. Rev. D* **101**, 022003 (2020), arXiv:1901.02227 [gr-qc].

- [53] B. Allen, W. G. Anderson, P. R. Brady, D. A. Brown, and J. D. E. Creighton, *Phys. Rev. D* **85**, 122006 (2012), arXiv:gr-qc/0509116.
- [54] K. Cannon, S. Caudill, C. Chan, B. Cousins, J. D. E. Creighton, B. Ewing, H. Fong, P. Godwin, C. Hanna, S. Hooper, R. Huxford, R. Magee, D. Meacher, C. Messick, S. Morisaki, D. Mukherjee, H. Ohta, A. Pace, S. Privitera, I. de Ruiter, S. Sachdev, L. Singer, D. Singh, R. Tapia, L. Tsukada, D. Tsuna, T. Tsutsui, K. Ueno, A. Viets, L. Wade, and M. Wade, *SoftwareX* **14**, 100680 (2021), arXiv:2010.05082 [astro-ph.IM].
- [55] P. Godwin *et al.*, (2020), arXiv:2010.15282 [gr-qc].
- [56] C. Chan, K. Cannon, S. Caudill, H. Fong, P. Godwin, C. Hanna, S. Kapadia, R. Magee, D. Meacher, C. Messick, S. R. Mohite, S. Morisaki, D. Mukherjee, A. Nishizawa, H. Ohta, A. Pace, S. Sachdev, M. Shikachi, L. Singer, L. Tsukada, D. Tsuna, T. Tsutsui, and K. Ueno, arXiv e-prints, arXiv:2009.03025 (2020), arXiv:2009.03025 [astro-ph.IM].
- [57] D. Mukherjee, S. Caudill, R. Magee, C. Messick, S. Privitera, S. Sachdev, K. Blackburn, P. Brady, P. Brockill, K. Cannon, *et al.*, *Physical Review D* **103**, 084047 (2021).
- [58] C. Messick, S. Sachdev, K. Cannon, S. Caudill, C. Chan, J. D. E. Creighton, R. Everett, B. Ewing, H. Fong, P. Godwin, C. Hanna, R. Huxford, S. Kapadia, A. K. Y. Li, R. K. L. Lo, R. Magee, D. Meacher, S. R. Mohite, D. Mukherjee, A. Nishizawa, H. Ohta, A. Pace, A. Reza, M. Shikachi, L. Singer, D. Singh, J. Rana SK, L. Tsukada, D. Tsuna, T. Tsutsui, K. Ueno, and A. Zimmerman, arXiv e-prints, arXiv:2011.02457 (2020), arXiv:2011.02457 [astro-ph.IM].
- [59] J. Veitch *et al.*, *Phys. Rev. D* **91**, 042003 (2015), arXiv:1409.7215 [gr-qc].
- [60] G. Ashton *et al.*, *Astrophys. J. Suppl. Ser.* **241**, 27 (2019), arXiv:1811.02042 [astro-ph.IM].
- [61] I. M. Romero-Shaw *et al.*, *Mon. Not. Roy. Astron. Soc.* **499**, 3295 (2020), arXiv:2006.00714 [astro-ph.IM].
- [62] G. Ashton and C. Talbot, *Mon. Not. Roy. Astron. Soc.* **507**, 2037 (2021), arXiv:2106.08730 [gr-qc].
- [63] H. K. Y. Fong, *From Simulations to Signals: Analyzing Gravitational Waves from Compact Binary Coalescences*, Ph.D. thesis, Department of Physics, University of Toronto (2018).
- [64] K. Cannon, C. Hanna, and J. Peoples, arXiv e-prints, arXiv:1504.04632 (2015), arXiv:1504.04632 [astro-ph.IM].
- [65] G. Pratten *et al.*, *Phys. Rev. D* **103**, 104056 (2021), arXiv:2004.06503 [gr-qc].
- [66] R. Abbott *et al.* (LIGO Scientific, VIRGO, KAGRA), “GWTC-3: Compact Binary Coalescences Observed by LIGO and Virgo During the Second Part of the Third Observing Run — Parameter estimation data release,” (2021), LIGO Laboratory and Advanced LIGO are funded by the United States National Science Foundation (NSF) as well as the Science and Technology Facilities Council (STFC) of the United Kingdom, the Max-Planck-Society (MPS), and the State of Niedersachsen/Germany for support of the construction of Advanced LIGO and construction and operation of the GEO600 detector. Additional support for Advanced LIGO was provided by the Australian Research Council. Virgo is funded, through the European Gravitational Observatory (EGO), by the French Centre National de Recherche Scientifique (CNRS), the Italian Istituto Nazionale di Fisica Nucleare (INFN) and the Dutch Nikhef, with contributions by institutions from Belgium, Germany, Greece, Hungary, Ireland, Japan, Monaco, Poland, Portugal, Spain. The construction and operation of KAGRA are funded by Ministry of Education, Culture, Sports, Science and Technology (MEXT), and Japan Society for the Promotion of Science (JSPS), National Research Foundation (NRF) and Ministry of Science and ICT (MSIT) in Korea, Academia Sinica (AS) and the Ministry of Science and Technology (MoST) in Taiwan.
- [67] M. Vallisneri, J. Kanner, R. Williams, A. Weinstein, and B. Stephens, in *Journal of Physics Conference Series*, Journal of Physics Conference Series, Vol. 610 (2015) p. 012021, arXiv:1410.4839 [gr-qc].